Joint Diseases and Related Surgery

Jt Dis Relat Surg
2025;36(1):97-106

ORIGINAL ARTICLE

Quantitative analysis of protective Kirschner wire diameters in lateral opening wedge distal femoral osteotomy: A finite element study

Alican Baris, MD[1], Emre Özmen, MD[1], Esra Circi, MD[1], Serdar Yuksel, MD[1], Ozan Beytemür, MD[2]

[1]Department of Orthopedics and Traumatology, İstanbul Physical Medicine and Rehabilitation Training and Research Hospital, İstanbul, Türkiye
[2]Department of Orthopedics and Traumatology, Bağcılar Training and Research Hospital, İstanbul, Türkiye

ABSTRACT

Objectives: This study aims to investigate quantitatively the protective effect of a 1.6-mm or a 2.5-mm Kirschner wire (K-wire) on the medial hinge at different gap distances through finite element analysis (FEA) and to establish whether using a 2.5-mm K-wire can offer benefits compared to a 1.6-mm in preventing medial hinge fractures.

Materials and methods: Between June 2024 and July 2024, three different models simulating a lateral opening wedge (LOW) osteotomy of the distal femur were created from a femoral computed tomography (CT) scan of a 36-year-old male patient: no K-wire (Model I), 1.6-mm K-wire (Model II), and 2.5-mm K-wire (Model III). Finite element analysis was performed to simulate 7- to 13-mm gaps at the osteotomy site. Loads, principal stress, strain, and equivalent stress were analyzed around the medial hinge.

Results: Model I required 123.0±5.2 N, Model II required 181.7±12.2 N, and Model III required 228.7±13.6 N ($p<0.001$). Cracked shell elements were the lowest in Model II and the highest in Model I. While the average equivalent/yield stress ratio was not significantly lower in Model II compared to Model III (87.0±10.9% *vs*. 92.7±12.1%), the maximum equivalent/yield stress ratio values in Model II were significantly lower than both Model I and Model III (1206.2±138.3% *vs*. 1836.2±165.4% and 1689.1±404.0%, respectively), suggesting a superior dispersion of forces.

Conclusion: Using a 1.6-mm K-wire during LOW osteotomy of the distal femur provides a balance between structural reinforcement and stress distribution, significantly improving stability and reducing the risk of medial hinge fractures compared to a 2.5-mm K-wire or no K-wire. The 1.6-mm K-wire optimizes stress dispersion, making it the preferred choice for surgical planning in lateral opening wedge distal femoral osteotomy.

Keywords: Biomechanics, distal femoral osteotomy, finite element analysis, hinge fracture, protective K-wire.

Valgus deformity of the distal femur affects the biomechanics of the lower extremity by creating an unfavorable mechanical alignment.[1] It is more common in women and it usually originates from a hypoplastic lateral femoral condyle. Its correction is indicated in patient where lateral compartment symptoms dominate the clinical picture.[2]

Distal femur lateral opening wedge (LOW) osteotomy or distal femur varus osteotomy (DFVO) is a common surgical technique used in the treatment of valgus malalignment of the distal femur.[3] Medial hinge fracture is one of the complications of this technique. As with other opening wedge osteotomies, the preservation of the hinge is critical for the stability of the osteotomy. Winkler et al.[4] recently classified medial hinge fractures in which the fracture line type 1 is an extension of the osteotomy, type 2 is a distally directed extension, and type 3 is a proximally directed extension.

Received: June 02, 2024
Accepted: September 17, 2024
Published online: November 05, 2024

Correspondence: Alican Baris, MD. İstanbul Fizik Tedavi ve Rehabilitasyon Eğitim ve Araştırma Hastanesi, Ortopedi ve Travmatoloji Kliniği, 34180 Bahçelievler, İstanbul, Türkiye.

E-mail: dralicanbaris@gmail.com

Citation: Baris A, Özmen E, Circi E, Yuksel S, Beytemür O. Quantitative analysis of protective Kirschner wire diameters in lateral opening wedge distal femoral osteotomy: A finite element study. Jt Dis Relat Surg 2025;36(1):97-106. doi: 10.52312/jdrs.2025.1806.

©2025 All right reserved by the Turkish Joint Diseases Foundation

This is an open access article under the terms of the Creative Commons Attribution-NonCommercial License, which permits use, distribution and reproduction in any medium, provided the original work is properly cited and is not used for commercial purposes (http://creativecommons.org/licenses/by-nc/4.0/).

Some biomechanical research has been published recently regarding the effects of osteotomy parameters such as inclination, end-point and gap distance on the hinge fractures.[5] Similar to opening wedge high tibial osteotomy (OWHTO),[6] one suggested method for preventing hinge fractures is using protective Kirschner wires (K-wires). A recent study by Mereb et al.[7] investigated the effect of high and low speed distraction with or without K-wires concerning maximum displacement, maximum breaking-point force and maximum time to fracture in three-dimensional (3D)-printed femora. To the best of our knowledge, no further biomechanical or finite element analysis (FEA) research has been carried out on this subject regarding the effects of various K-wire diameters, as well as quantitative analysis on the hinge region during osteotomy opening.

The finite element method (FEM) is a technique used for simulating the physical behavior of structures under load. It involves breaking down a complex problem into smaller, simpler parts called finite elements called nodes, and creating a mesh that represents the physical shape of the object or area under study. By incorporating known properties and conditions into this mesh, FEM allows for the calculation of factors such as stress, strain, and displacement within the structure.[8]

In the present study, we aimed to investigate quantitatively the protective effect of a 1.6-mm or a 2.5-mm K-wire on the medial hinge at different gap distances through FEA and to establish whether using a 2.5-mm K-wire could offer benefits compared to a 1.6-mm in preventing medial hinge fractures.

MATERIALS AND METHODS

This experimental study was conducted at İstanbul Physical Therapy and Rehabilitation Training and Research Hospital, Department of Orthopedics and Traumatology between June 2024 and July 2024. A written informed consent was obtained from the patient. The study protocol was approved by the İstanbul Physical Medicine and Rehabilitation Training and Research Hospital Institutional Review Board (IRB) (date: 28.05.2024, no: 2024-35). The study was conducted in accordance with the principles of the Declaration of Helsinki.

A previously obtained distal femoral computed tomography (CT) scan with 1-mm cuts of a 36-year-old male patient, performed for trauma investigation purposes unrelated to the current study, was used for the model. Mechanical Finder version 12.0 (Research Center for Computational Mechanics, Tokyo, Japan) was used to segment the CT scan and create the bone mesh. Mesh convergence test suggested 2.0-mm mesh size for the bone model to be optimal for this study, consistent with the literature.[9] The outer surface of the mesh consisted of triangular elements, whereas the inside consisted of tetrahedral elements. The average number of nodes was 46,807, shells 22,333, and solids 226,082. A shell with a thickness of 0.3 was added to the surface. The Poisson's ratio for each element was set at 0.4. A rectangular chisel with a thickness of 2 mm, as well as 1.6- and 2.5-mm K-wires were designed in SpaceClaim R17.0 software (ANSYS) with a mesh size of 0.8 mm.

The chisel was placed starting approximately 3 cm above the lateral femoral epicondyle and angled medially and distally toward the base of the medial

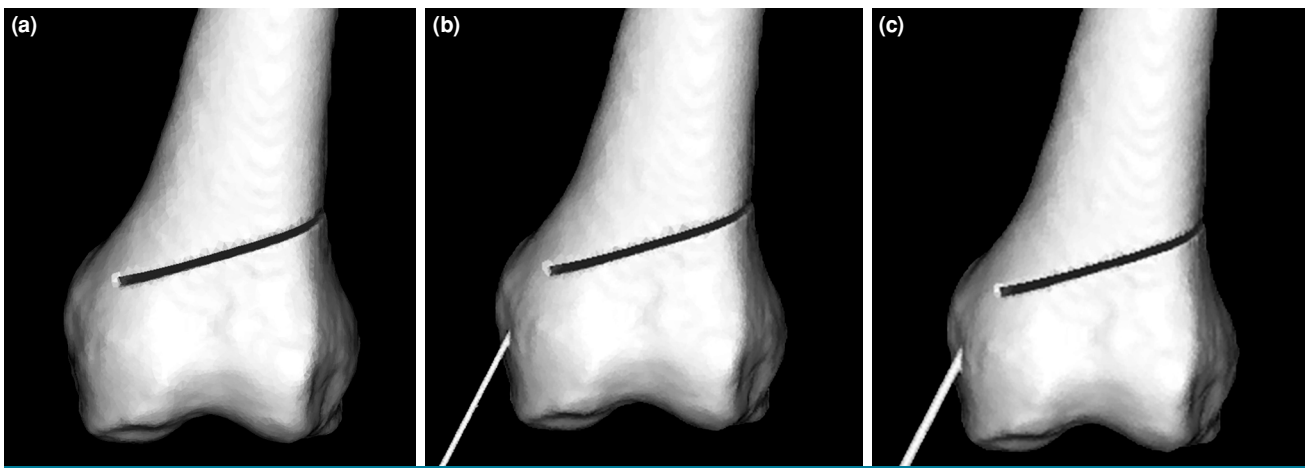


FIGURE 1. (a) Base osteotomy model. **(b)** Osteotomy model with a 1.6-mm K-wire. **(c)** Osteotomy model with a 2.5-mm K-wire.

femoral condyle, just above the medial epicondyle. A 1-cm medial bone bridge was maintained for stability. The intersection area between the chisel and the bone was extracted from the model to simulate the osteotomy (Model I) (Figure 1a).[10] Two additional models with 1.6 mm (Model II) and 2.5 K-wires (Model III) were, then, prepared in the same manner with K-wires (Figure 1b and c). The K-wires were positioned in the middle of the anteroposterior plane and directed craniocaudally, through the center of the hinge and exiting distal to the medial epicondyle.[7,11] The material properties of the K-wires were assigned with Poisson's ratio of 0.3, and Young's modulus of 186.400 MPa.[12] The average ash density for each bone element was determined based on the mean ash density of the voxels within that element.[13] The Young's modulus and yield stress for each isotropic tetrahedral element were derived using the formulas suggested by Keyak et al.[14,15]

$$\text{BMD } (g/cm^3)=(\text{CT value [H.U.]} + 1.4246) \times 0.001/1.058$$

Figure 2 shows the density map of the distal femur on laid on the CT scan.

Loading and boundary conditions were set by fixing the model 15 cm proximal to the joint line and applying the load at the lateral cortex at a 90-degree angle, in a similar fashion to an osteotomy distractor (Figure 3). Different loads were empirically applied to deform the models so that 7- to 13-mm gaps (in addition to the gap caused by the chisel) were created. The Drucker-Prager equivalent criterion was adopted for the yield of the elements.[16] After the simulation, volumetric and surface analysis were done at the medial hinge region (Figure 4), by extracting the maximum and average values in the region of interest regarding maximum principal stress, maximum principal strain, equivalent stress, maximum principal/critical stress (%) and equivalent/yield stress (%). The values from the nodes representing the K-wire were omitted during this analysis.

Statistical analysis

Statistical analysis was performed using the IBM SPSS version 27.0 software (IBM Corp., Armonk, NY, USA). Descriptive data were expressed in mean ± standard deviation (SD), median (min-max) or number and frequency, where applicable. The distribution of variables was checked using the

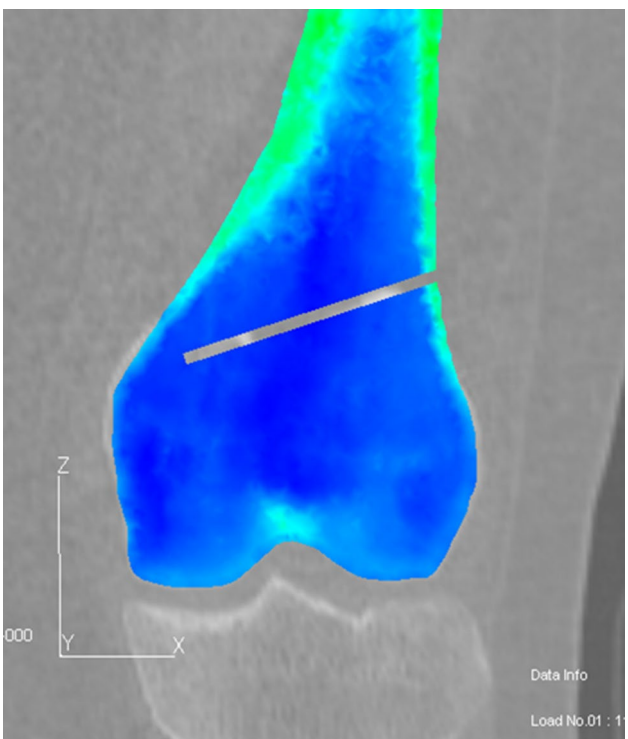


FIGURE 2. Graphical representation of Young's modulus of the individual elements on top of the corresponding computed tomography slice.



FIGURE 3. Loading and boundary conditions. Distal femur was fixed at the proximal end and load was applied perpendicularly at the osteotomy site.

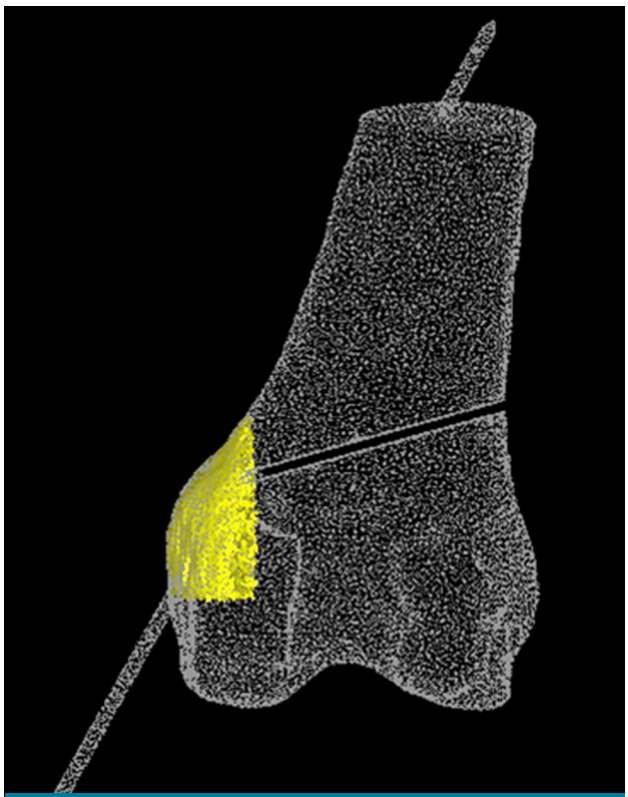


FIGURE 4. Region of interest at the hinge area to extract biomechanical data.

Kolmogorov-Smirnov test. Independent samples t-test and Mann-Whitney U test were used for the comparison of quantitative data. A *p* value of <0.05 was considered statistically significant.

RESULTS

The mean maximum and average solid principal stresses were 210.9±63.3 MPa and 3.83±0.59 MPa, while the mean maximum and average solid principal strains were 0.53±0.46 and 0.02±0.01. For shell elements, the mean maximum and average principal stresses were 515.9±153.1 MPa and 22.0±3.1 MPa, and the mean maximum and average principal strains were 0.38±0.30 and 0.01±0.00, respectively.

The mean force required to open the osteotomy site significantly differed among model types, with Model I requiring 123.0±5.2 N, Model II requiring 181.7±12.2 N, and Model III requiring 228.7±13.6 N (p<0.001). The mean percent of cracked shell elements was the lowest in Model II (1.01±0.13%) and the highest in Model I (1.63±0.17%). Similarly, cracked solid elements were significantly different among the models, with Model I showing the least (1.07±0.14%) and Model III the most (1.95±0.19%). Additionally, the number of plastic and crushed solid elements was significantly lower in type 1 compared to Model II and III (p<0.001) (Table I).

Stress and strain analysis of solid elements

Significant differences in solid principal stress, strain, and equivalent stress were observed among the model types (Table II).

The mean maximum solid principal strain was the highest in Model II (0.64±0.80) and the lowest in Model III (0.38±0.07) (p=0.012), while the average solid principal strain was the highest in Model III (0.0195±0.0046) and the lowest in Model I (0.0111±0.0019) (p=0.001). The maximum solid principal stress was the highest in Model III (264.1±62.9 MPa) and the lowest in Model I (152.0±21.7 MPa) (p=0.004). The average solid principal stress was the highest in Model III (4.22±0.32 MPa) and the lowest in Model II (3.09±0.25 MPa) (p<0.001) (Figude 5a). The average solid principal/critical

TABLE I
Comparison of finite element analysis results for shell and solid elements across models

	Model I (Base)			Model II (1.6 mm K-wire)			Model III (2.5 mm K-wire)			
	n	Mean±SD	Median	n	Mean±SD	Median	n	Mean±SD	Median	*p*
Nodes	39142			42993			50621			
Shells	22166			22153			22513			
Solids	189784			207996			244168			
Force (MPa)		123.0±5.2	123.5		181.7±12.2	183.0[1]		228.7±13.6	229.0[1]	<0.001†
Cracked shells (%)		1.63±0.17	1.63		1.01±0.13	1.00[1]		1.19±0.15	1.19[1]	<0.001†
Cracked solids (%)		1.07±0.14	1.07		1.95±0.19	1.95[1]		1.70±0.15	1.70[1]	<0.001†
Plastic solids (%)		0.16±0.03	0.16		1.36±0.03	0.16[1]		1.22±0.16	1.22[1]	<0.001†
Crushed solids (%)		0.09±0.03	0.09		0.71±0.14	0.71[1]		0.70±0.14	0.70[1]	<0.001†

SD: Standard deviation; [1] Difference with Model I group p<0.05; † ANOVA test.

TABLE II
Comparison of strain and stress results for solid elements across models

	Model I[1]		Model II[2]		Model III[3]		
	Mean±SD	Median	Mean±SD	Median	Mean±SD	Median	*p*
Solid principal stress (MPa)							
Max	152.0±21.7	143.4[32]	216.6±39.1	225.2	264.1±62.9	274.6	0.004‡
Ave	4.17±0.26	4.19	3.09±0.25	3.07[31]	4.22±0.32	4.34	<0.001†
Solid principal strain							
Max	0.57±0.09	0.57[2]	0.64±0.80	0.35	0.38±0.07	0.38[1]	0.012‡
Ave	0.0111±0.0019	0.012[32]	0.0188±0.0037	0.0186	0.0195±0.0046	0.0190	0.001†
Solid principal/critical stress ratio							
Max	679.4±172.3	793.8	552.2±163.2	497.2	575.0±104.2	636.3	0.299‡
Ave	34.9±2.1	34.7[3]	37.2±1.5	36.9[3]	42.2±2.2	42.6	<0.001†
Solid equivalent stress (MPa)							
Max	195.4±27.5	183.6[32]	267.7±46.3	284.2	320.6±75.5	330.9	0.005‡
Ave	8.7±0.5	8.7[3]	8.4±0.7	8.3[3]	11.2±0.8	11.4	<0.001†
Solid equivalent/yield stress ratio							
Max	1836.2±165.4	1800.3	1206.2±138.3	1220.7[13]	1689.1±404.0	1792.0	0.001†
Ave	53.8±4.3	54.8[23]	87.0±10.9	86.3	92.7±12.1	93.9	<0.001†

SD: Standard deviation; † ANOVA test; ‡ Kruskal-Wallis (Mann-Whitney U test); [1] Difference with Model I group p<0.05; [2] Difference with Model II group p<0.05; [3] Difference with Model III group p<0.05.

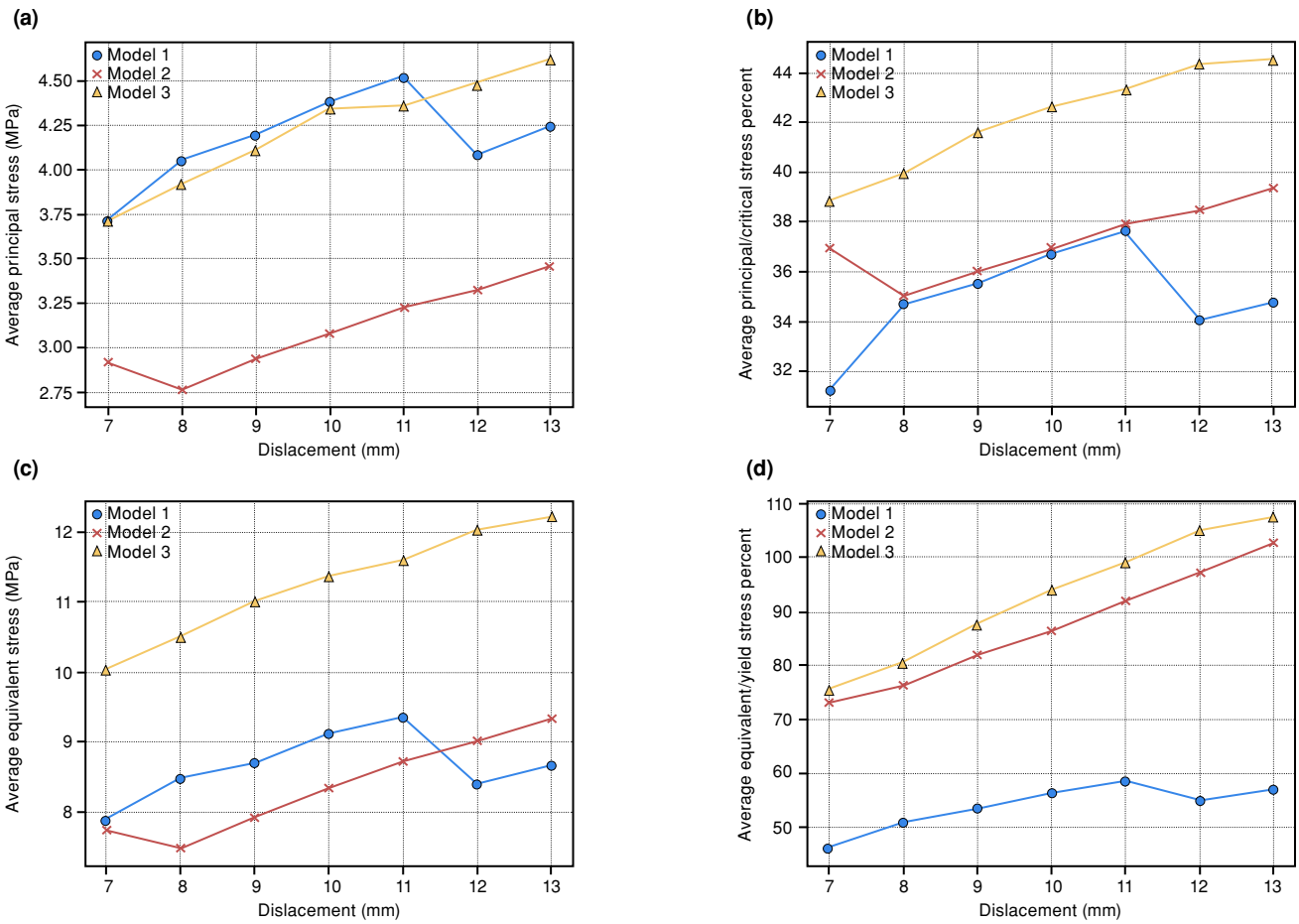


FIGURE 5. Results for solid elements. **(a)** Average principal stress at each gap distance. **(b)** Average principal/critical stress percent at each distance. **(c)**Average equivalent stress at each gap distance. **(d)** Average equivalent/yield stress percent at each distance.

TABLE III
Comparison of strain and stress results for shell elements across models

	Model I[1]		Model II[2]		Model III[3]		
	Mean±SD	Median	Mean±SD	Median	Mean±SD	Median	*p*
Solid principal stress (MPa)							
Max	461.5±89.7	439.7[3]	402.9±110.0	399.9[3]	683.3±83.4	652.5	<0.001†
Ave	24.7±2.0	25.7	18.3±1.7	18.4[13]	23.1±0.8	23.0	<0.001†
Solid principal strain							
Max	0.37±0.06	0.35[2]	0.38±0.53	0.18[3]	0.39±0.11	0.43	0.029‡
Ave	0.01±0.00	0.01	0.01±0.00	0.00	0.01±0.00	0.01	0.202†
Solid principal/critical stress ratio							
Max	135.6±44.9	128.4	113.4±17.1	100.0	107.2±11.6	105.0	0.519‡
Ave	18.0±0.4	18.0	14.7±1.2	14.4[13]	16.2±0.7	16.4[1]	<0.001†
Solid equivalent stress (MPa)							
Max	612.6±127.5	587.4[3]	542.2±131.2	555.2[3]	922.7±118.1	882.0	<0.001†
Ave	79.9±1.2	79.6[32]	81.0±0.9	81.2[3]	85.0±1.7	84.9	<0.001‡
Solid equivalent/yield stress ratio							
Max	294.4±61.3	282.2[3]	260.5±62.9	266.7[3]	443.3±56.6	424.1	<0.001†
Ave	46.2±2.1	46.9[3]	48.6±3.2	49.0[3]	57.2±3.1	57.0	<0.001†

SD: Standard deviation; † ANOVA test; ‡ Kruskal-Wallis (Mann-Whitney U test); [1] Difference with Model I group p<0.05; [2] Difference with Model II group p<0.05; [3] Difference with Model III group p<0.05.

stress percentage showed significant differences, with Model III having the highest percentage (42.2±2.2%) and Model I the lowest (34.9±2.1%) (p<0.001) (Figure 5b). The maximum solid equivalent stress was the highest in Model III (320.6±75.5 MPa) and the lowest in Model I (195.4±27.5 MPa) (p=0.005), with the average solid equivalent stress being the highest in Model III (11.2±0.8 MPa) and the lowest in Model II (8.4±0.7 MPa) (p<0.001) (Figure 5c). Finally, the maximum solid equivalent/yield stress percentage was the highest in Model I (1836.2±165.4%) and the lowest in Model II (1206.2±138.3%) (p=0.001), while the average solid equivalent/yield stress percentage was the highest in Model III (92.7±12.1%) and the lowest in Model I (53.8±4.3%) (p<0.001) (Figure 5d).

Shell elements analysis

Significant differences in shell principal stress, strain, and equivalent stress were found among the model types (Table III). The maximum shell principal stress was the highest in Model III (683.3±83.4 MPa) and the lowest in Model II (402.9±110.0 MPa) (p<0.001), with the average shell principal stress being the highest in Model I (24.7±2.0 MPa) and lowest in Model II (18.3±1.7 MPa) (p<0.001) (Figure 6a). The maximum shell principal/critical percentage showed no significant differences among models (p=0.519), but the average shell principal/critical percentage was significantly lower in Model II (14.7±1.2%) compared to Models I and III (p<0.001) (Figure 6b). The maximum shell principal strain showed significant variation, with Model III exhibiting the highest (0.39±0.11) and Model II the lowest (0.38±0.53) (p=0.029). Although the average shell principal strain did not show significant differences (p=0.202), the maximum shell equivalent stress was notably the highest in Model III (922.7±118.1 MPa) and the lowest in Model II (542.2±131.2 MPa) (p<0.001). The average shell equivalent stress was the highest in Model III (85.0±1.7 MPa) and the lowest in Model I (79.9±1.2 MPa) (p<0.001) (Figure 6c). Additionally, the maximum shell equivalent/yield stress percentage was significantly the highest in Model III (443.3±56.6%) and the lowest in Model II (260.5±62.9%) (p<0.001), with the average shell equivalent/yield stress percentage being the highest in Model III (57.2±3.1%) and the lowest in Model I (46.2±2.1%) (p<0.001) (Figure 6d).

DISCUSSION

Lateral opening wedge distal femoral osteotomy (LOWDFO) is a useful procedure for correcting

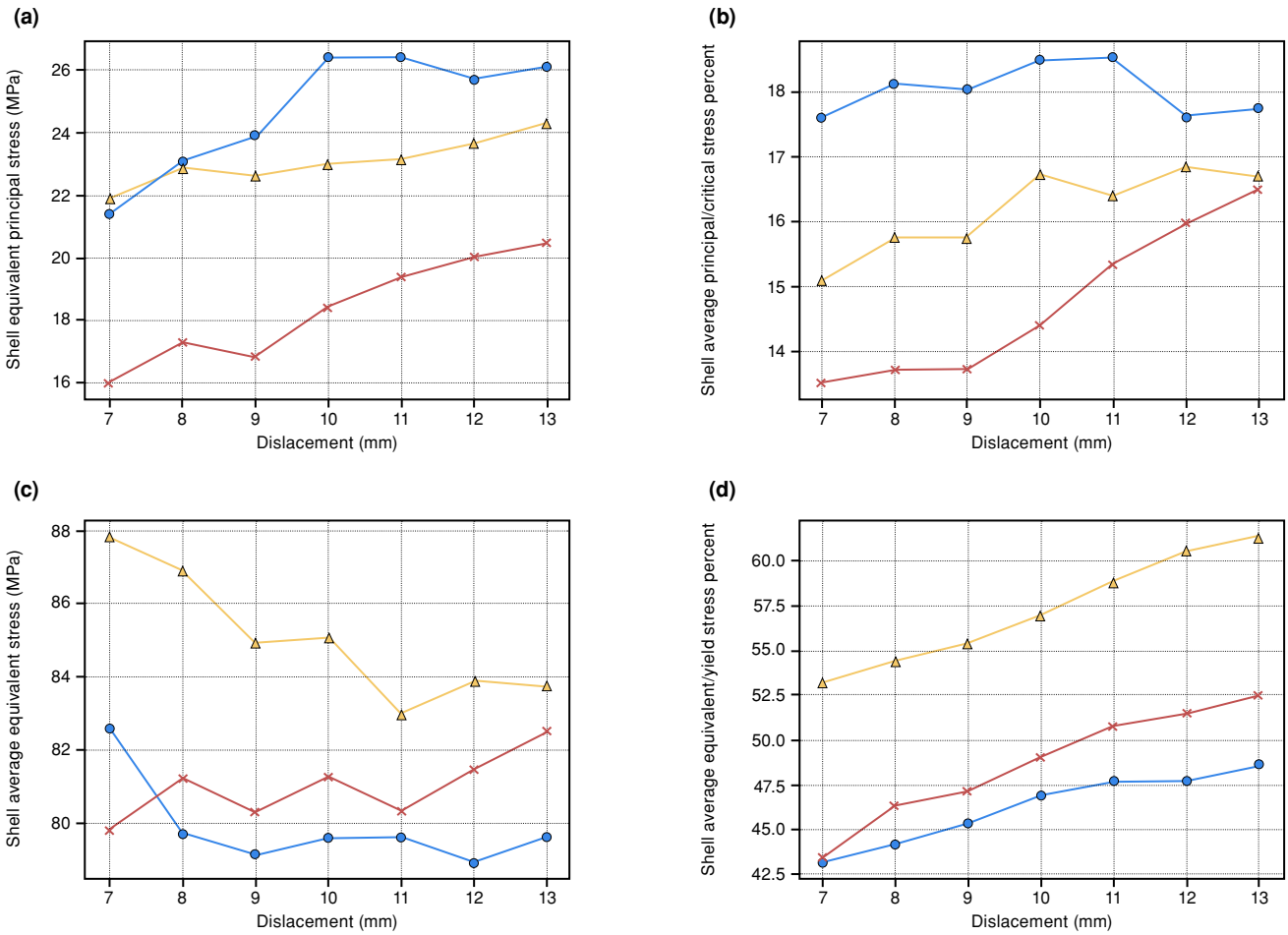


FIGURE 6. Results for shell elements. **(a)** Average principal stress at each gap distance for shell elements. **(b)** Average principal/critical stress percent at each distance shell elements. **(c)** Average equivalent stress at each gap distance shell elements. **(d)** Average equivalent/yield stress percent at each distance shell elements.

the mechanical alignment of the lower extremity in valgus malalignment. Conserving the medial hinge is critical to ensure the stability of the osteotomy.[1] The medial hinge fracture is a recognized complication of the procedure and a protective K-wire at the hinge site is a proposed solution to this problem.

In the current study, we investigated the protective effect of a 1.6-mm or a 2.5-mm K-wire on the medial hinge at different gap distances through FEA. Our study results demonstrated significant differences in the force required to open the osteotomy site among various models, with Model III requiring the highest force. This is expected, since thicker K-wires make the construct stiffer. Similarly, the increased shell element failures observed in Model III can be attributed to the higher forces required to distract the osteotomy.

Examining both principal and equivalent stresses provides a better understanding of the stress distributions and potential failure points within the bone and the protective K-wires. Principal stress analysis highlights the maximum normal stresses which are crucial for identifying areas prone to fracture. Equivalent stress, on the other hand, combines the effects of all stress components, offering a holistic view of the material's response to complex loading conditions. If the equivalent stress is greater than the yield stress, the element gets plastic deformation. Figure 7 illustrates visually the dispersing of equivalent stress around the hinge with a K-wire. The principal/critical stress ratio helps to identify areas prone to fracture by focusing on maximum normal stresses, while the equivalent/yield stress ratio provides an overall

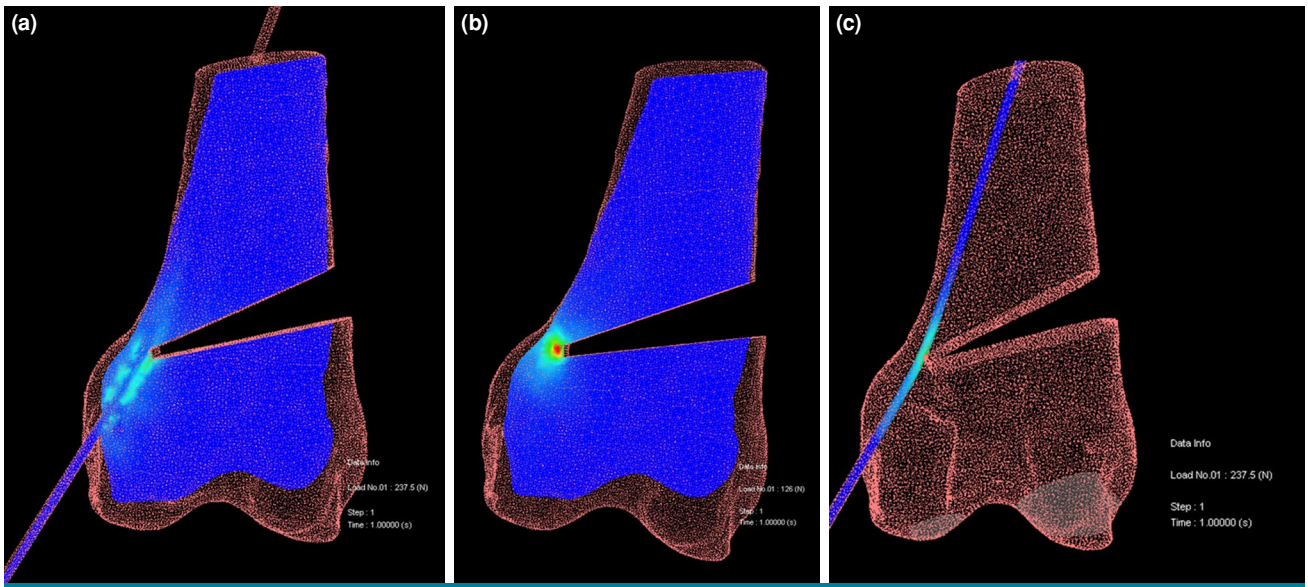


FIGURE 7. Visualization of the protection of a K-wire at the hinge site. **(a)** Tensile forces are dispersed around the wire. **(b)** No K-wire results in concentrated stresses. **(c)** Tensile stresses on the K-wire.

view of the risk of plastic deformation by combining all stress components.

A higher principal/critical percentage indicates that the material is under greater stress relative to its capacity to withstand that stress without yielding. Furthermore, a ratio exceeding 100% suggests the risk of hinge fracture.[17] In inhomogeneous materials, the equivalent/yield stress ratio can be a more reliable indication than scalar units.

Shell elements were used in this study to accurately study the surface stresses. Unlike solid elements, which have tetrahedral shapes, shell elements are two-dimensional (2D) triangles with pre-determined thicknesses placed on the surface solid. They help to compensate for the CT resolution at regions with thin cortices, such as the distal metaphyseal region.

Our results indicate that with a thicker K-wire, more force is required the open the osteotomy site. The 1.6-mm K-wire model required on average 58.7 N more force than the base model, and the 2.5-mm K-wire model required on average 105.7 N more force than the base model. However, by analyzing the cracked shell elements, the results were surprising in the sense that the 1.6 K-wire model had decreased percent of cracked shells compared to the base model, and the 2.5-mm K-wire model was not superior to the 1.6 K-wire model in decreasing cracked shell elements. Indeed, the number of cracked shells was on average greater in 2.5-mm K-wire model. We suggest that this may be due to the increased force required to open the osteotomy site. The K-wire protects the hinge at the midsagittal part of the distal femur, with increased force to open the osteotomy site, the increase in tensile forces anterior and posteriorly may offset the advantages gained by using a thicker K-wire.

For the tetrahedral elements, the FEA data revealed that the 1.6-mm K-wire model exhibited advantages in terms of lower principal stress than other models and similar average principal/critical stress percent compared to the base model. In terms of the equivalent stress, the 1.6-mm K-wire model had similar average equivalent stress values to the base model. More intriguingly, increasing the K-wire thickness to 2.5 seems to offer no advantages in terms of decreasing principal and equivalent stresses, and the results in significantly more average principal/critical stress percent ratios across the board.

Review of the literature reveals several studies investigating the role of protective K-wires in reducing hinge fractures in tibial osteotomies. A study by Gulagaci et al.[18] demonstrated that positioning a K-wire to intersect the cutting plane at the theoretical lateral hinge location significantly reduced the occurrence of perioperative hinge fractures during medial OWHTO. The authors reported that patients with a K-wire had a lower lateral hinge fracture

(LHF) rate (16.7%) compared to those without a K-wire (43.3%). Similarly, Didier et al.[19] investigated the impact of K-wires in high tibial osteotomies, noting their protective benefits during the osteotomy procedure. Their study showed that the presence of a K-wire significantly increased the load to failure and maximum displacement, indicating enhanced stability and resistance to fracture. Regarding femoral osteotomies, a recent study by Mereb et al.[7] reported biomechanical data on the protective effect of a K-wire. Notably, only a single K-wire size was used (2 mm) and 3D-printed femurs were used for this study. The authors also simulated the trabecular and cortical bone by printing the fibers at certain orientations; however, FEA as in this study using CT data may be a more favorable representation of the actual bone quality, since the mechanical properties of the bone are assigned at a voxel-by-voxel basis.

Nonetheless, there are some limitations to this study. The main limitation is related to the generalizability of the results in the broader orthopedic context due to the use of a single CT scan of a healthy adult, as well as the lack of validation studies of this model in cadaver studies. With regards to the use of a single CT scan, FEA offers a significant advantage in drawing meaningful conclusions with small sample sizes, as it allows testing the same model under various conditions, in this case using 21 different models (7 for each model). On the other hand, while other cadaveric validation studies of CT based FEA analysis using Mechanical Finder were performed on proximal femur,[20] femoral shaft,[13] distal radius[21] and vertebrae,[22] and to the best of our knowledge, there is no study to validate a specific distal femoral osteotomy model.

On the other hand, our results indicate that a K-wire may be protective in preventing medial hinge fractures. This is the first study to examine quantitatively the effects and studying different-sized K-wires.[23]

In conclusion, our study results showed significant differences in the equivalent/yield stress ratio among models of LOWDFO using K-wires of varying diameters. Based on these findings, we suggest that, despite similar average equivalent/yield stress ratio values, Model II disperses the forces acting on the medial hinge more effectively, as indicated by its significantly lower maximum equivalent/yield stress ratio values. This balance provides structural reinforcement while mitigating the risk of localized plastic deformation, making Model II a viable option for enhancing stability in clinical applications. Further large-scale, well-designed studies are needed to draw more reliable conclusions on this subject.

Acknowledgements: During the preparation of this study the authors used ChatGPT (OpenAI, San Francisco, CA, USA) in for grammar and syntax editing. After using this tool/service, the authors reviewed and edited the content as needed and take full responsibility for the content of the publication. The final manuscript was reviewed by a professional translator.

Data Sharing Statement: The data that support the findings of this study are available from the corresponding author upon reasonable request.

Author Contributions: Idea/concept, writing the article: E.Ö., A.B.; Design: E.Ö., A.B., O.B.; Control/supervision: S.Y.; Data collection and/or processing: E.Ö., A.B., S.Y; Analysis and/or interpretation, references and fundings, materials: E.Ö.; Literature review: E.C., E.Ö; Critical review: E.C., S.Y., O.B.

Conflict of Interest: The authors declared no conflicts of interest with respect to the authorship and/or publication of this article.

Funding: The authors received no financial support for the research and/or authorship of this article.

REFERENCES

1. Liu XY, Yu QP, Chen XM, Zeng WN, Zhou ZK. Effects of preoperative valgus deformity in patients undergoing neutrally aligned total knee arthroplasty: A retrospective cohort study with a minimum five-year follow-up. Jt Dis Relat Surg 2024;35:529-37. doi: 10.52312/jdrs.2024.1800.
2. Cameron JI, McCauley JC, Kermanshahi AY, Bugbee WD. Lateral opening-wedge distal femoral osteotomy: Pain relief, functional improvement, and survivorship at 5 years. Clin Orthop Relat Res 2015;473:2009-15. doi: 10.1007/s11999-014-4106-8.
3. Matsuoka M, Kondo E, Iwasaki K, Onodera T, Nakamura R, Nakayama H, et al. Simultaneous medial closing wedge distal femoral varus osteotomy and double-bundle anterior cruciate ligament reconstruction in the symptomatic femoral valgus deformity: A case report. Jt Dis Relat Surg 2024;35:422-32. doi: 10.52312/jdrs.2023.1176.
4. Winkler PW, Rupp MC, Lutz PM, Geyer S, Forkel P, Imhoff AB, et al. A hinge position distal to the adductor tubercle minimizes the risk of hinge fractures in lateral open wedge distal femoral osteotomy. Knee Surg Sports Traumatol Arthrosc 2021;29:3382-91. doi: 10.1007/s00167-020-06244-6.
5. Meisterhans M, Flury A, Zindel C, Zimmermann SM, Vlachopoulos L, Snedeker JG, et al. Finite element analysis of medial closing and lateral opening wedge osteotomies of the distal femur in relation to hinge fractures. J Exp Orthop 2023;10:33. doi: 10.1186/s40634-023-00597-w.
6. Koh DTS, Soong J, Yeo W, Tan MWP, Teo SJ, Wilson A, et al. Large versus small opening wedge high tibial osteotomies performed with a protective wire over the lateral hinge: Incidence of lateral hinge fracture and early clinical outcomes. Am J Sports Med 2023;51:672-7. doi: 10.1177/03635465221148496.
7. Mereb T, Favreau H, Ollivier M, Jmal H, Bonnomet F, Bahlouli N, et al. Experimental study of risk of medial hinge fracture during distal femoral varus osteotomy. Orthop Traumatol Surg Res 2023;109:103527. doi: 10.1016/j.otsr.2022.103527.

8. Heller MO. Finite element analysis in orthopedic biomechanics. In: Innocenti B, Galbusera F, editors. Human orthopaedic biomechanics: Fundamentals, devices and applications. Cambridge: Elsevier; 2022. p. 637-58.
9. Morita Y, Kuriyama S, Maeda T, Nakamura S, Nishitani K, Ito H, et al. Hinge fractures reaching the tibial plateau can be caused by forcible opening of insufficient posterior osteotomy during open-wedge high tibial osteotomy. Knee Surg Sports Traumatol Arthrosc 2023;31:1533-45. doi: 10.1007/s00167-021-06816-0.
10. Jacquet C, Chan-Yu-Kin J, Sharma A, Argenson JN, Parratte S, Ollivier M. "More accurate correction using "patient-specific" cutting guides in opening wedge distal femur varization osteotomies. Int Orthop 2019;43:2285-91. doi: 10.1007/s00264-018-4207-1.
11. Teo SJ, Koh DTS, Soong JW, Yeo W, Wilson A, Lee KH. Distalization of hinge site with use of hinge wire reduces hinge fracture rates in closing wedge distal femoral osteotomy. Knee Surg Sports Traumatol Arthrosc 2023;31:3141-50. doi: 10.1007/s00167-022-07286-8.
12. Kim Y, Kwon M, Ryu JY, Moon SW. Biomechanical analysis of the Kirschner-wire depth of the modified tension band wiring technique in transverse patellar fractures: An experimental study using the finite-element method. Clin Orthop Surg 2021;13:315-9. doi: 10.4055/cios20253.
13. Wako Y, Nakamura J, Matsuura Y, Suzuki T, Hagiwara S, Miura M, et al. Finite element analysis of the femoral diaphysis of fresh-frozen cadavers with computed tomography and mechanical testing. J Orthop Surg Res 2018;13:192. doi: 10.1186/s13018-018-0898-7.
14. Keyak JH, Rossi SA, Jones KA, Skinner HB. Prediction of femoral fracture load using automated finite element modeling. J Biomech 1998;31:125-33. doi: 10.1016/s0021-9290(97)00123-1.
15. Keyak JH, Lee IY, Skinner HB. Correlations between orthogonal mechanical properties and density of trabecular bone: Use of different densitometric measures. J Biomed Mater Res 1994;28:1329-36. doi: 10.1002/jbm.820281111.
16. Drucker DC, Prager W. Soil mechanics and plastic analysis or limit design. Q Appl Mat1952;10:157-65.
17. Kuwashima U, Itoh M, Itou J, Okazaki K. Impact of support instruments in medial closed-wedge distal femoral osteotomy: A finite element analysis. Arch Orthop Trauma Surg 2024;144:1039-45. doi: 10.1007/s00402-023-05152-x.
18. Gulagaci F, Jacquet C, Ehlinger M, Sharma A, Kley K, Wilson A, et al. A protective hinge wire, intersecting the osteotomy plane, can reduce the occurrence of perioperative hinge fractures in medial opening wedge osteotomy. Knee Surg Sports Traumatol Arthrosc 2020;28:3173-82. doi: 10.1007/s00167-019-05806-7.
19. Didier A, Favreau H, Ollivier M, Jmal H, Bonnomet F, Bahlouli N, et al. Experimental investigation of the risk of lateral cortex fracture during valgus tibial osteotomy. Orthop Traumatol Surg Res 2022;108:103428. doi: 10.1016/j.otsr.2022.103428.
20. Miura M, Nakamura J, Matsuura Y, Wako Y, Suzuki T, Hagiwara S, et al. Prediction of fracture load and stiffness of the proximal femur by CT-based specimen specific finite element analysis: cadaveric validation study. BMC Musculoskelet Disord 2017;18:536. doi: 10.1186/s12891-017-1898-1.
21. Yamazaki T, Matsuura Y, Suzuki T, Ohtori S. Evaluation of fixation after plating of distal radius fractures - a validation study. Comput Methods Biomech Biomed Engin 2021;24:1687-92. doi: 10.1080/10255842.2021.1909576.
22. Imai K. Analysis of vertebral bone strength, fracture pattern, and fracture location: A validation study using a computed tomography-based nonlinear finite element analysis. Aging Dis 2015;6:180-7. doi: 10.14336/AD.2014.0621.
23. Atik OŞ. Writing for Joint Diseases and Related Surgery (JDRS): There is something new and interesting in this article! Jt Dis Relat Surg 2023;34:533. doi: 10.52312/jdrs.2023.57916.